Inorganic Chemistry
Article

Inorg. Chem. **2009,** *48,* 5039–5046 **5039**
DOI:10.1021/ic900384n

Formation and Interconversion of Organo-Cobalt Complexes in Reactions of Cobalt(II) Porphyrins with Cyanoalkyl Radicals and Vinyl Olefins

Chi-How Peng,[†] Shan Li,[†] and Bradford B. Wayland*[,‡]

[†]*Department of Chemistry, University of Pennsylvania, Philadelphia, Pennsylvania 19104-6323, and*
[‡]*Department of Chemistry, Temple University, Philadelphia, Pennsylvania 19122*

Received February 24, 2009

Observation of the formation and interconversion of organo-cobalt complexes ((TMP)Co-R) is used to reveal mechanistic features in the living radical polymerization (LRP) of methyl acrylate (MA) mediated by cobalt porphyrins. Both dissociative and associative exchange of radicals in solution with organo-cobalt complexes contribute to controlling the radical polymerization. The sequence of organo-cobalt species formed during the induction period for the (TMP)Co-R mediated LRP of MA indicates that homolytic dissociation is a prominent pathway for the interconversion of organo-cobalt complexes which contrasts with the corresponding vinyl acetate (VAc) system where associative radical exchange totally dominates these processes. The dissociation equilibrium constant ($K_{d(333\ K)}$) for organo-cobalt complexes formed in methyl acrylate polymerization ((TMP)Co-CH(CO_2CH_3)CH_2P) was estimated as 1.15×10^{-10} from analysis of the polymerization kinetics and ^{1}H NMR. The ratio of the rate constants (333 K) for the cyanoisopropyl radical (•C$(CH_3)_2$CN) adding with monomer (k_1) to the process of transferring a hydrogen atom to (TMP)Co^{II}• (k_2) was evaluated for the methyl acrylate system as 2×10^{-3} which is larger than that for vinyl acetate LRP (9×10^{-5}). Kinetic analysis places the rate constant for associative radical interchange (333 K) at $\sim 7 \times 10^5$ M^{-1} s^{-1}. The larger radical stabilization energy and lower energy of the singly occupied molecular orbital (SOMO) for methyl acrylate based radicals (•CH(CO_2CH_3)CH_2P) compared to vinyl acetate contribute to the observed prominence of organo-cobalt homolytic dissociation and much smaller chain transfer which result in substantially better control for living radical polymerization of methyl acrylate than that observed for vinyl acetate.

Introduction

Reactions of organic carbon-centered radicals with cobalt-centered radicals and organo-cobalt complexes provide several mechanisms to achieve living radical polymerization (LRP).[1−21] The most prominent metal site reactions that occur when organic radicals interact with cobalt-centered radicals and organo-cobalt species in solution are shown in Scheme 1.[22,23] When an organic radical (•C(CH_3)(R)X) encounters cobalt-centered radicals (Co•) in solution a solvent caged radical pair (Co••C(CH_3)(R)X) is formed which either collapses to form an organo-cobalt complex (Co-C(CH_3)(R)X), or reacts by Co• abstracting a β-hydrogen from the radical (•C(CH_3)(R)X) to form a cobalt hydride

*To whom correspondence should be addressed. E-mail: bwayland@temple.edu.

(1) Wayland, B. B.; Poszmik, G.; Mukerjee, S. L.; Fryd, M. *J. Am. Chem. Soc.* **1994**, *116*, 7943–7944.
(2) Lu, Z.; Fryd, M.; Wayland, B. B. *Macromolecules* **2004**, *37*, 2686–2687.
(3) Wayland, B. B.; Peng, C.-H.; Fu, X.; Lu, Z.; Fryd, M. *Macromolecules* **2006**, *39*, 8219–8222.
(4) Peng, C.-H.; Fryd, M.; Wayland, B. B. *Macromolecules* **2007**, *40*, 6814–6819.
(5) Peng, C.-H.; Scricco, J.; Li, S.; Fryd, M.; Wayland, B. B. *Macromolecules* **2008**, *41*, 2368–2373.
(6) Li, S.; de Bruin, B.; Peng, C.-H.; Fryd, M.; Wayland, B. B. *J. Am. Chem. Soc.* **2008**, *130*, 13373–13381.
(7) Poli, R. *Angew. Chem., Int. Ed.* **2006**, *45*, 5058–5070.
(8) Maria, S.; Kaneyoshi, H.; Matyjaszewski, K.; Poli, R. *Chem.—Eur. J.* **2007**, *13*, 2480–2492.
(9) Tsarevsky, N. V.; Matyjaszewski, K. *Chem. Rev.* **2007**, *107*, 2270–2299.
(10) Wang, J. S.; Matyjaszewski, K. *J. Am. Chem. Soc.* **1995**, *117*, 5614–5615.
(11) Wakioka, M.; Baek, K.-Y.; Ando, T.; Kamigaito, M.; Sawamoto, M. *Macromolecules* **2002**, *35*, 330–333.
(12) Kato, M.; Kamigaito, M.; Sawamoto, M.; Higashimura, T. *Macromolecules* **1995**, *28*, 1721–1723.
(13) Debuigne, A.; Caille, J-R.; Jèrôme, R. *Angew. Chem., Int. Ed.* **2005**, *44*, 1101–1104.
(14) Debuigne, A.; Willet, N.; Jèrôme, R.; Detrembleur, C. *Macromolecules* **2007**, *40*, 7111–7118.
(15) Debuigne, A.; Warnant, J.; Jèrôme, R.; Voets, I.; De Keizer, A.; Cohen Stuart, M. A.; Detrembleur, C. *Macromolecules* **2008**, *41*, 2353–2360.
(16) Debuigne, A.; Michaux, C.; Jérôme, C.; Jérôme, R.; Poli, R.; Detrembleur, C. *Chem.—Eur. J.* **2008**, *14*, 7623–7637.
(17) Debuigne, A.; Poli, R.; Jérôme, C.; Jérôme, R.; Detrembleur, C. *Prog. Polym. Sci.* **2009**, *34*, 211–239.
(18) Asandei, A. D.; Moran, I. W. *J. Am. Chem. Soc.* **2004**, *126*, 15932–15933.
(19) Asandei, A. D.; Saha, G. *Macromolecules* **2006**, *39*, 8999–9009.
(20) Goto, A.; Kwak, Y.; Fukuda, T.; Yamago, S.; Iida, K.; Nakajima, M.; Yoshida, J. *J. Am. Chem. Soc.* **2003**, *125*, 8720–8721.
(21) Langlotz, B. K.; Fillol, J. L.; Gross, J. H; Wadepohl, H.; Gade, L. H. *Chem. Eur. J.* **2008**, *14*, 10267–10279.
(22) Halpern, J. *Polyhedron* **1988**, *7*, 1483–1490.
(23) Ng, F. T. T.; Rempel, G. L.; Mancuso, C.; Halpern, J. *Organometallics* **1990**, *9*, 2762–2772.

Published on Web 5/7/2009

Scheme 1. Reactions of Cobalt-Centered Radicals and Organo-Cobalt Complexes with Organic Radicals

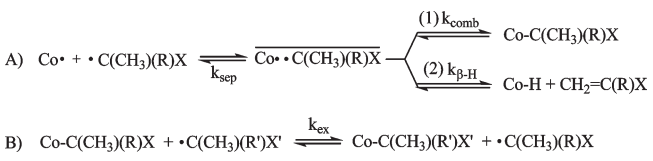

(Co−H) and an olefin (CH_2=C(R)X) (Scheme 1(A)).[22] Exchange of organic radicals in solution with latent organic fragments in organo-cobalt species is depicted in Scheme 1(B).[5,6,8,16]

Reversible bond homolysis and radical exchange of organo-cobalt complexes (Scheme 1(A1),(B)) are respectively used in mediating living radical polymerization by reversible termination (RT)[2,5,24−26] and degenerative transfer (DT)[5,6,27−29] pathways (eqs 1, 2). Cobalt porphyrin complexes accomplish each type of the reactions with organic radicals shown in Scheme 1[1−6,30−34] and have been observed to mediate LRP by both RT and DT pathways (eqs 1, 2).

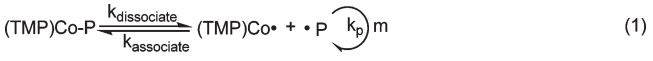

(1)

(2)

This article reports on the formation and interconversion of organo-cobalt complexes during the methyl acrylate living radical polymerization mediated by cobalt porphyrin complexes and the results are compared with the vinyl acetate system. ^{1}H NMR studies and kinetic simulations were used to establish the reaction scheme and evaluate the thermodynamic and kinetic parameters for the methyl acrylate LRP. The stabilization energy for the monomer radical of MA (•$CH(CO_2CH_3)CH_3$) and VAc (•$CH(OC(O)CH_3)CH_3$) and the energy of the singly occupied molecular orbital (SOMO) were computed by density functional theory (DFT) calculations and used in explaining mechanistic differences between MA and VAc living radical polymerizations.

Results and Discussion

Cobalt Porphyrin Mediated Living Radical Polymerization of Methyl Acrylate. Representative first-order kinetic plots for living radical polymerization of MA using (TMP)Co^{II}• (**1**) as the catalyst and varying quantities of

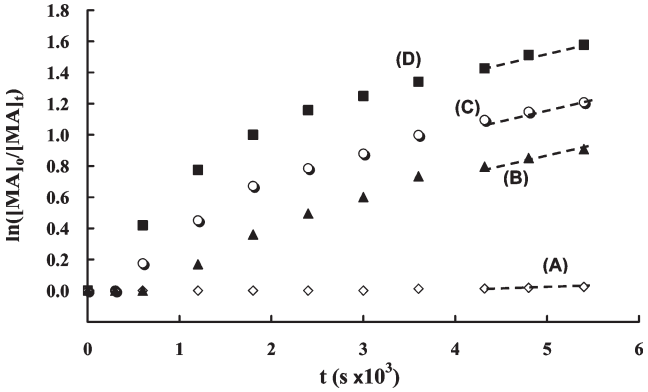

Figure 1. Kinetic plots for polymerization of methyl acrylate (MA) in C_6D_6 at 333 K initiated by V-70 with $[(TMP)Co^{II}•]_i = 1.0 \times 10^{-3}$ M, $[MA]_i = 2.25$ M, $[V\text{-}70]_i/[(TMP)Co^{II}•]_i$ = (A) 0.53; (B) 1.21; (C) 1.58; (D) 2.54, slope of the dotted line = (A) 5×10^{-4} s^{-1}; (B) 8.2×10^{-3} s^{-1}; (C) 8.1×10^{-3} s^{-1}; (D) 8.3×10^{-3} s^{-1}.

V-70 ($[((CH_3)_2(CH_3O)CCH_2)(CN)(CH_3)C]_2N_2$) as an azo radical source are shown in Figure 1. The half-life for V-70 at 333 K in benzene is 10.2 min[35] so that within 1.0 to 1.5 h V-70 is fully expended. Radical polymerization of MA at the conditions where the total moles of radicals that enter solution from V-70 exceed the initial moles of (TMP)Co^{II}• is illustrated in Figure 1B−D. An induction period where only a few percent of monomer conversion to polymer occurs followed by the onset of rapid polymerization after most of the (TMP)Co^{II}• has been converted to organo-cobalt complexes, (TMP)Co-P. At the early stage of polymerization, dissociation of both the organo-cobalt complex and the initiator are radical sources. When the external radical source (V-70) is exhausted, the polymerization rate decreases because dissociation of organo-cobalt complex ((TMP)Co-P) becomes the exclusive radical source ($[P•] = K_{dissociation(333\ K)}$ [(TMP)Co-P]/[(TMP)Co^{II}•]). This is a defining feature for a RT living radical polymerization process which is also referred to a dissociation combination (DC) pathway. The radicals in solutions are maintained at a near constant low concentration by a quasi-equilibrium with the dormant organo-cobalt complex (eq 1). This condition is experimentally manifested by the parallel linear regions of the first order rate plots that occur when all of the V-70 radical source has dissociated (Figure 1B−D). The observed rate of polymerization in this region corresponds to the rate that would be obtained from using a pure organo-Co(TMP) complex to initiate and control the polymerization. Comparable polymerizations of vinyl acetate initiated by V-70 controlled by (TMP)Co species produced qualitatively similar results[5] but after all of the V-70 is consumed, the polymerization virtually stopped because of the extremely small extent of Co−R bond homolysis in the vinyl acetate polymerization system.

Near linear growth in molecular weight and relatively low polydispersity as the MA conversion increases (Figure 2) illustrate the living character of the polymerization process. Control of the radical polymerization

(24) Matyjaszewski, K.; Xia, J. H. *Chem. Rev.* **2001**, *101*, 2921–2990.
(25) Kamigaito, M.; Ando, T.; Sawamoto, M. *Chem. Rev.* **2001**, *101*, 3689–3746.
(26) Yoshikawa, C.; Goto, A.; Fukuda, T. *Macromolecules* **2003**, *36*, 908–912.
(27) Iovu, M. C.; Matyjaszewski, K. *Macromolecules* **2003**, *36*, 9346–9354.
(28) Chiefari, J.; Chong, Y. K.; Ercole, F.; Krstina, J.; Jeffery, J.; Le, T. P. T.; Mayadunne, R. T. A.; Meijs, G. F.; Moad, C. L.; Moad, G.; Rizzardo, E. *Macromolecules* **1998**, *31*, 5559–5562.
(29) Moad, G.; Rizzardo, E.; Thang, S. H. *Aust. J. Chem.* **2005**, *58*, 379–410.
(30) Gridnev, A. A.; Ittel, S. D. *Chem. Rev.* **2001**, *101*, 3611–3660.
(31) Li, Y.; Wayland, B. B. *Chem. Commun.* **2003**, 1594–1595.
(32) Tang, L.; Norton, J. R. *Macromolecules* **2006**, *39*, 8229–8235.
(33) Stoffelbach, F.; Poli, R.; Maria, S.; Richard, P. *J. Organomet. Chem.* **2007**, *692*, 3133–3143.
(34) Allan, L. E. N.; Shaver, M. P.; White, A. J. P.; Gibson, V. C. *Inorg. Chem.* **2007**, *46*, 8963–8970.
(35) (a) Table of Azo Polymerization initiators provided by Wako Chemicals U.S.A., Inc.(b) Dixon, K. W. In *Polymer Handbook*, 4th ed.; Brandrup, J., Immergut, E. H., Grulke, E. A., Ed.; Wiley: New York, 1999; p II/1.

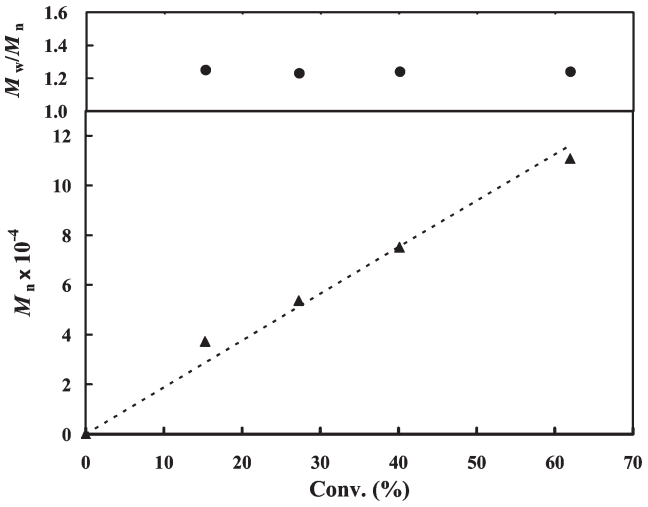

Figure 2. Change in the number average molecular weight (M_n) and polydispersity (M_w/M_n) with conversion of methyl acrylate (MA) to polymethyl acrylate (PMA) at 333 K in C_6D_6. $[MA]_i$ = 2.2 M; $[(TMP)Co^{II}\bullet]_i = 1.0 \times 10^{-3}$ M; $[V\text{-}70]_i = 1.1 \times 10^{-3}$ M. The dotted line represents the theoretical behavior for one polymer chain per organocobalt complex.

during the post induction period when rapid polymerization occurs is provided by a degenerative transfer (DT) mechanism where radicals ($[R\bullet] = (k_i[V\text{-}70]/2k_t)^{1/2}$) entering solution from V-70 adds to monomer to both initiate polymerization and exchange with dormant radicals in the (TMP)Co-P complex (eq 2). After the external radical source (V-70) is fully dissociated, all of the radicals in solution result from dissociation of the organometallic complex, and the control of the radical polymerization occurs by the RT mechanism (eq 1). Similar results were obtained for VAc polymerization at low monomer conversion, but chain transfer causes deviations from ideality that increases with conversion.[5]

The rate of the living radical polymerization process mediated by excess of $(TMP)Co^{II}\bullet$ (**1**) provides an approach to evaluate the equilibrium constant (K_d) for dissociation of methyl acrylate based organo-cobalt porphyrin complexes (eq 3). Three independent polymerization

$$(TMP)Co-CH(CO_2CH_3)CH_2-P \overset{k_d}{\rightleftharpoons} (TMP)Co\bullet + \bullet CH(CO_2CH_3)CH_2-P \quad (3)$$

reactions of methyl acrylate were mediated by $(TMP)Co^{II}\bullet$ (1.0×10^{-3} M) where the total moles of initiator radicals entering solution are less than the initial moles of $(TMP)Co^{II}\bullet$ (Figure 3). ^{1}H NMR was used to follow the reactions and evaluate the ratio of $(TMP)Co^{II}\bullet$ to (TMP)Co-CH$(CO_2CH_3)CH_2$-P by comparing integrations of the *m*-phenyl hydrogen resonance for $(TMP)Co^{II}\bullet$ (δ = 9.33 ppm, s) and the pyrrole hydrogen resonance for (TMP)Co-CH$(CO_2CH_3)CH_2$-P (δ = 8.79 ppm, dd, AB). The concentration of organic radicals in solution is derived from the slope of the first order rate plot ($[R\bullet]$ = Slope/k_p) along with knowledge of the propagation constant of methyl acrylate ($k_p = 1.3 \times 10^4$ M^{-1} s^{-1} at 333 K).[36] Direct evaluation of the dissociation equilibrium

(36) Moad, G.; Rizzardo, E.; Solomon, D. H.; Beckwith, A. L. J. *Polym. Bull.* **1992**, *29*, 647–652.

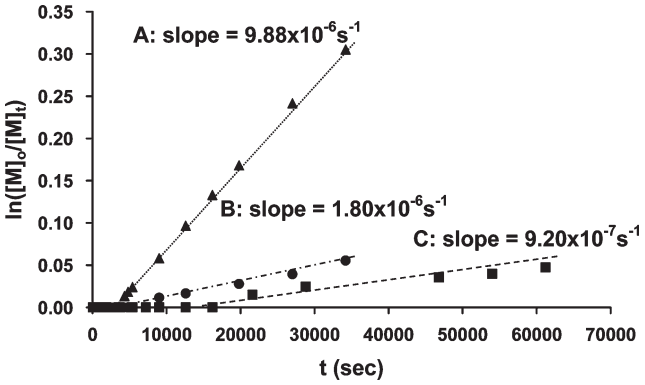

Figure 3. Kinetic plots for polymerization of methyl acrylate (MA) in C_6D_6 at 333 K initiated by V-70 with $[(TMP)Co^{II}\bullet]_i = 1.0 \times 10^{-3}$ M, (A) $[V\text{-}70]_i/[(TMP)Co^{II}\bullet]_i$ = 0.7, $[MA]_i$ = 2.2 M; (B) $[V\text{-}70]_i/[(TMP)Co^{II}\bullet]_i$ = 0.5, $[MA]_i$ = 2.2 M; (C) $[V\text{-}70]_i/[(TMP)Co^{II}\bullet]_i$ = 0.4, $[MA]_i$ = 0.8 M.

Table 1. Evaluation of the (TMP)Co-P Dissociation Equilibrium Constant (Kd) at 333 K in C_6D_6

data	slope (s^{-1})	[radical] (M)	[Co(II)]/[Co-P]	$K_{d(333\ K)}$
A	9.88×10^{-6}	7.60×10^{-10}	0.138	1.1×10^{-10}
B	1.80×10^{-6}	1.38×10^{-10}	0.850	1.2×10^{-10}
C	9.20×10^{-7}	7.07×10^{-11}	1.740	1.2×10^{-10}

constant for (TMP)Co-P (K_d = $[P\bullet][(TMP)Co^{II}\bullet]/[(TMP)Co\text{-}P]$) for these three independent MA polymerizations yield an average K_d of $1.15 \pm 0.10 \times 10^{-10}$ at 333 K (Table 1). Efforts to evaluate the dissociation constant ($K_{d(333\ K)}$) for the analogous vinyl acetate organometallic complex (TMP)Co-CH$(OC(O)CH_3)CH_2$-P were unsuccessful because the extent of dissociation was too small to give finite rates of polymerization.

The (TMP)Co-CH$(CO_2CH_3)CH_2$-P dissociation constant affects the shape of the polymerization rate plots. Simulation of the polymerization rate plots using rate constants given in the Supporting Information is fully consistent with the measured (TMP)Co-CH$(CO_2CH_3)CH_2$-P dissociation constant of 1.15×10^{-10} at 333 K (Figure 4).

Formation and Transformation of Organo-Cobalt Complexes. Formation of the organometallic species during the course of cobalt porphyrin mediated radical polymerization of methyl acrylate using azo radical sources is conveniently followed by ^{1}H NMR in both the pyrrole hydrogen region (δ = 8.77 ~ 8.93 ppm; Figure 5) and the high field region where groups attached to the cobalt center often appear (δ = 0 ~ −6 ppm; Figure 6).

During the induction period prior to rapid MA polymerization, paramagnetic $(TMP)Co^{II}\bullet$ (**1**) is converted to diamagnetic organo-cobalt porphyrin complexes, and the time evolution is followed by changes in the porphyrin ^{1}H NMR (Figure 5). The relatively broad peak at δ = 9.36 ppm is for porphyrin *m*-phenyl hydrogens of paramagnetic $(TMP)Co^{II}\bullet$, and the narrow AB patterned doublet of doublet at δ = 8.85 ppm are for porphyrin pyrrole hydrogens for diamagnetic (TMP)Co-PMA complexes. The hydrogens on adjacent porphyrin pyrrole carbon centers of (TMP)Co-PMA (**5**) become inequivalent through the presence of chiral carbon centers in the organo group bonded to cobalt ((TMP)Co-C*H(X)CH_2-P). The ester group on the α-carbon in (TMP)Co-CH$(CO_2CH_3)CH_2$-P is primarily responsible

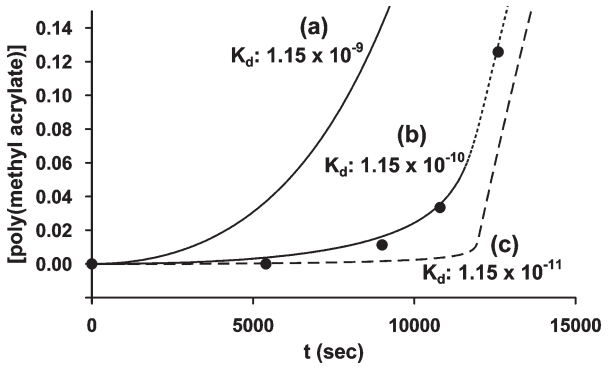

Figure 4. Simulation of the polymerization rate plot for methyl acrylate (1.1 M) mediated by (TMP)Co^{II}• (5.9×10^{-4} M) and initiated by AIBN (7.6×10^{-3} M) (●) at 333 K. Solid dots are the observed data points and lines are the kinetic simulation lines with K_d = (a) 1.15×10^{-9}; (b) 1.15×10^{-10}; (c) 1.15×10^{-11} (simulation details are in the Supporting Information).

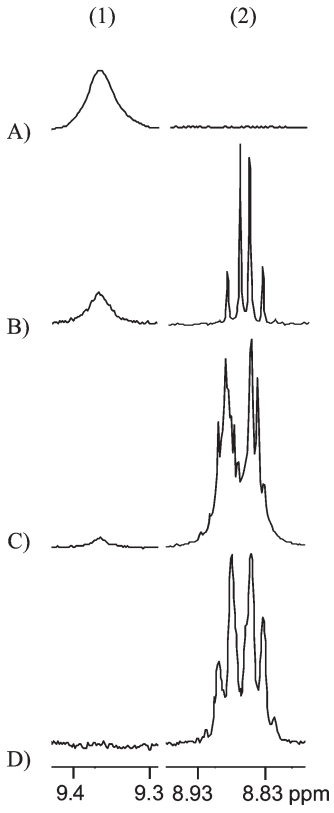

Figure 5. Changes in ^{1}H NMR (500 MHz, C_6D_6) for cobalt porphyrins as a function of time through the induction period of MA polymerization at 313 K. (1) *m*-phenyl hydrogens of paramagnetic (TMP)Co^{II}•, (2) pyrrole hydrogens of diamagnetic organo-Co(TMP) complexes. Initial concentrations: $[(TMP)Co^{II}•]_i = 1.48 \times 10^{-3}$ M, $[V\text{-}70]_i = 2.00 \times 10^{-3}$ M, $[MA]_i = 0.14$ M. (A) 0 min; (B) 100 min; (C) 200 min; (D) 300 min.

for a substantial chemical shift between adjacent pyrrole hydrogens which appear as an AB pattern in the ^{1}H NMR (Figure 5).

Four types of organo-cobalt complexes (TMP)Co-CH(CO_2CH_3)CH_2-C(CH_3)(R)CN (**2**, Co-MA-In), (TMP)Co-CH(CO_2CH_3)CH_3 (**3**, Co-MA), (TMP)Co-CH(CO_2CH_3)CH_2-CH(CO_2CH_3)CH_3 (**4**, Co-MA_2), and (TMP)Co-PMA (**5**, Co-MA_n) were observed during the induction period. During the time period when a substantial concentration of (TMP)Co^{II}• (**1**) remains in solution, complexes **2** and **3** are formed by reactions that compete for the cyanoalkyl radicals (•C(CH_3)(R)CN, •In) from thermal dissociation of V-70 (Scheme 2) (eqs 4−7). When the cyanoalkyl radical from an azo initiator reacts with a

$$CH_2{=}CH(CO_2CH_3) + •C(CH_3)(R)CN\ (•In) \xrightarrow{k_1} •CH(CO_2CH_3)CH_2{-}C(CH_3)(R)CN\ (•MA{-}In) \quad (4)$$

$$(TMP)Co• + •CH(CO_2CH_3)CH_2{-}C(CH_3)(R)CN \rightleftharpoons (TMP)Co{-}CH(CO_2CH_3)CH_2{-}C(CH_3)(R)CN\ (\mathbf{2}, Co{-}MA{-}In) \quad (5)$$

$$(TMP)Co• + •C(CH_3)(R)CN\ (•In) \overset{k_2}{\rightleftharpoons} [(TMP)Co{-}H] + CH_2{=}C(R)CN \quad (6)$$

$$[(TMP)Co{-}H] + CH_2{=}H(CO_2CH_3) \rightharpoonup (TMP)Co{-}CH(CO_2CH_3)CH_3\ (\mathbf{3}, Co{-}MA) \quad (7)$$

monomer olefin (CH_2=CH(CO_2CH_3), MA), a monomer carbon based radical •CH(CO_2CH_3)CH_2-C(CH_3)(R)CN (•MA-In) is formed (eq 4). Before •MA-In can propagate further with monomers it combines with (TMP)Co^{II}• by a near diffusion controlled reaction to produce the organometallic complex (TMP)Co-CH(CO_2CH_3)CH_2-C(CH_3)(R)CN (Co-MA-In, **2**) (eq 5). Only a small amount of **2** was observed by ^{1}H NMR during the V-70 initiated MA polymerization Figure 6(C), Supporting Information) because the reaction of •In with (TMP)Co^{II}• to form a cobalt hydride intermediate by β−H abstraction (eq 6) is a faster process in the range of MA concentrations studied. The reaction scheme shown in Scheme 2 was also observed in cobalt porphyrin mediated vinyl acetate polymerization and formation of the cobalt hydride intermediate is the more favorable pathway as well when V-70 was used as the initiator.[6] Addition of (TMP)Co-H to the double bond of methyl acrylate forms (TMP)Co-CH(CO_2CH_3)CH_3 (**3**) (eq 7) as the exclusive species observed in the ^{1}H NMR (Figure 6(B)). The same regioselectivity also occurs in VAc polymerization.[5,6]

The ratio of the rate constants (k_1/k_2) for the competing pathways that convert (TMP)Co^{II}• into organo-cobalt complexes **2** and **3** (Scheme 2(A), (B)) can be evaluated from the observed concentrations of **2** and **3** formed by each pathway.[6] The ratio of the concentrations of Co-MA-In to Co-MA ([**2**]/[**3**]) is observable by ^{1}H NMR at relatively high monomer concentrations ([MA] > 0.27 M) and low concentrations of (TMP)Co^{II}• ($[Co^{II}•] < 7.15 \times 10^{-4}$ M) which favor the production of **2**. The observed ratio of [**2**]/[**3**] at low conversion of (TMP)Co^{II}• to (TMP)Co-R along with the expression of [**2**]/[**3**] = k_1[R•][MA]/k_2[Co^{II}•][R•] = (k_1/k_2)([MA]/[Co^{II}•]) provides an estimate for the ratio of k_1 to k_2 as $k_1/k_{2(313\ K)} = 5 \times 10^{-4}$. Substituting V-70 by AIBN to initiate the MA polymerization at 333 K gives the value of k_1/k_2 equal to 2×10^{-3}. The value of k_1/k_2 is affected by both temperature and steric hindrance of the initiator.

Following the initial formation of **2** and **3**, more organo-cobalt complexes (**4** and **5**) form. The alternative

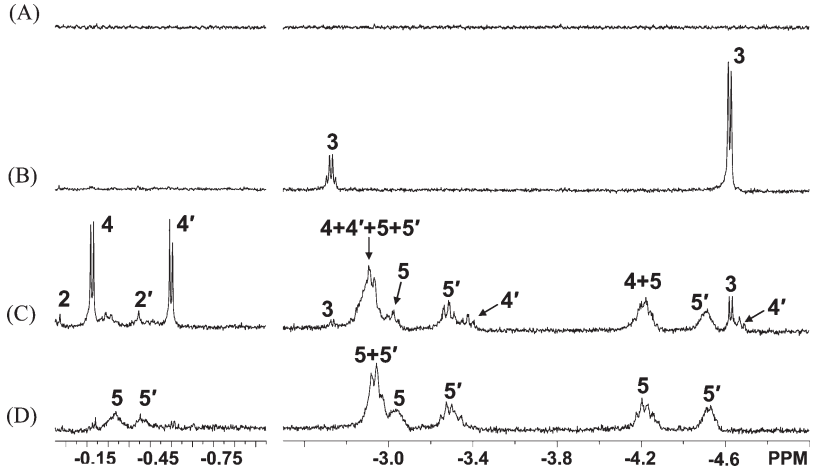

Figure 6. Changes in ^{1}H NMR (500 MHz, C_6D_6) high-field region for organo-cobalt complexes during the polymerization of methyl acrylate at 313 K. Initial concentrations: $[(TMP)Co^{II}\bullet]_i = 1.48 \times 10^{-3}$ M, $[V\text{-}70]_i = 2.00 \times 10^{-3}$ M, $[MA]_i = 0.14$ M. (A) 0 min; (B) 100 min; (C) 200 min; (D) 300 min. The NMR assignments of organo-cobalt species: (TMP)Co-CH(CO_2CH_3)CH_2-C(CH_3)(R)CN (**2**), (TMP)Co-CH(CO_2CH_3)CH_3 (**3**), (TMP)Co-CH(CO_2CH_3)CH_2CH(CO_2CH_3)CH_3 (**4**), and (TMP)Co-PMA (**5**) are provided in the Supporting Information.

Scheme 2. Alternative Reactions of Cyanoalkyl Radicals from V-70 with $(TMP)Co^{II}$ and Olefin Monomers

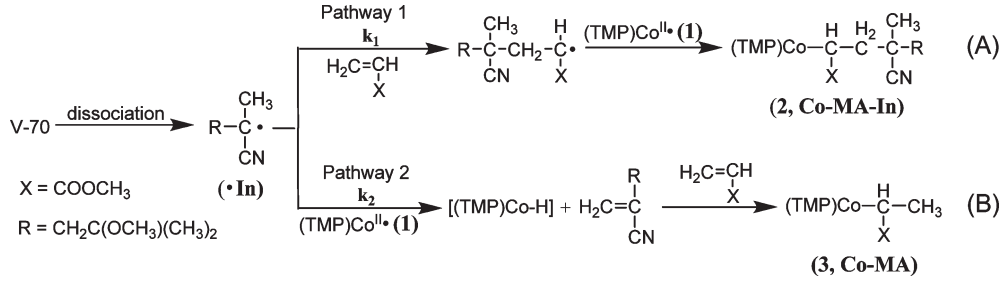

Scheme 3. Organometallic Formation and Transformation through RT and Degenerative Transfer (DT) Pathways in the Cobalt Porphyrin Mediated LRP of MA

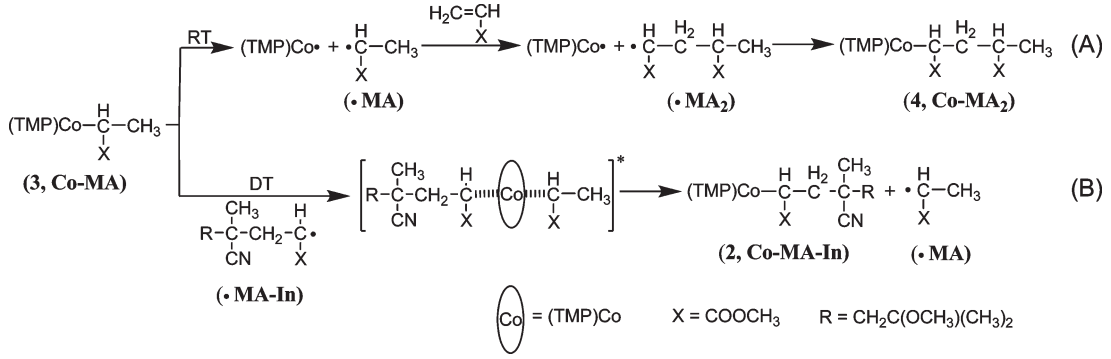

RT and degenerative transfer (DT) pathways that use (TMP)Co-CH(CO_2CH_3)CH_3 (**3**, Co-MA) to mediate living radical polymerization of MA are outlined in Scheme 3. Conversion of Co-MA (**3**) to Co-MA_2 (**4**) during the induction period results from the consecutive reactions of Co-MA bond homolysis (eq 8), MA propagation to form •MA_2 (eq 9), and the recombination with $(TMP)Co^{II}\bullet$ (eq 10). Repetition of this sequence of reactions results in a Co-MA mediated living radical polymerization of MA by a RT pathway. Initiator capped organo-cobalt complex results from reaction of the initiator radical (•In) with MA to form •MA-In (eq 11) followed by formation of Co-MA-In through either combination with $(TMP)Co^{II}\bullet$ (eq 12) or radical interchange with Co-MA (eq 13).

$$(TMP)Co{-}MA \rightleftharpoons (TMP)Co^{II}\bullet + \bullet MA \quad (8)$$

$$\bullet MA + MA \rightarrow \bullet MA_2 \quad (9)$$

$$(TMP)Co^{II}\bullet + \bullet MA_2 \rightleftharpoons (TMP)Co{-}MA_2 \quad (10)$$

$$\bullet In + MA \rightarrow \bullet MA{-}In \quad (11)$$

$$(TMP)Co\bullet + \bullet MA{-}In \rightleftharpoons (TMP)Co{-}MA{-}In \quad (12)$$

$$(TMP)Co{-}MA + \bullet MA{-}In \rightleftharpoons (TMP)Co{-}MA{-}In + \bullet MA \quad (13)$$

Two chiral centers of (TMP)Co-C*H(CO_2CH_3)CH_2C*H(CO_2CH_3)CH_3 (**4**, Co-MA_2) produce diastereomers with

two sets of hydrogen resonances in high field ^{1}H NMR region ($\delta = 0 \sim -6$ ppm). Observing the time evolution of the ^{1}H NMR spectrum permitted identifying the resonances associated with **4** (Figure 6). The prominent doublet resonances at −0.18 ppm and −0.55 ppm correspond to terminal -CH_3 group on the diastereomers. Complex **4** only occurs for a relatively short time before being converted to organo-cobalt complexes of poly(methyl acrylate), (TMP)Co-PMA (**5**). Two chiral centers close to the cobalt site in polymer-cobalt complexes also give two sets of hydrogen resonances in the high field region ($\delta = 0 \sim -6$ ppm) (Supporting Information). Although (TMP)Co-CH(CO_2CH_3)CH_2-CH(CO_2CH_3)CH_2-PMA (**5**) and (TMP)Co-CH(CO_2CH_3)CH_2-CH(CO_2CH_3)CH_3 (**4**) have the same first two MA units bonded to the cobalt center, their chemical shifts are slightly different. Larger steric demands of the polymer chain probably results in conformational changes reflected in the ^{1}H NMR.

The quantitative mechanistic analysis based on ^{1}H NMR observations and the kinetic model in Schemes 2 and 3 is shown in Figure 7. The set of reactions and corresponding rate constants used in the kinetic simulation are listed in the Supporting Information. The ^{1}H NMR resonances for Co-MA-In (**2**) are not large enough for quantitative analysis under the conditions of this study and thus only complexes **1**, **3**, **4**, **5** are considered in this quantitative mechanism analysis.

The radical exchange rates are not uniquely determined by the kinetic analysis, but reasonable fits of experimental data are only obtained when the rate constants for near degenerate radical interchange (eq 14−16) are greater than 4×10^5 M^{-1} s^{-1} and less than 1×10^6 M^{-1} s^{-1}. The fit between experiment and calculation given in Figure 7 is obtained when the radical exchange rate constants k_{14}, k_{15}, and k_{16} are equal to 7×10^5 M^{-1} s^{-1}. The rate constants deduced for radical exchange ($k_{ex(313\ K)} \sim 7 \times 10^5$ M^{-1} s^{-1}) ($R_m\bullet$ + (TMP)Co-R_n ⇌ R_m-Co(TMP) + $R_n\bullet$) in the (TMP)Co system are comparable to or larger than the values reported for radical exchange rates with dithioesters (RAFT)[28,37] and a series of organo-main group species[38−40] that are observed to control living radical polymerization by degenerative transfer. These radical exchange rate constants ($k_{ex(313\ K)} \sim 7 \times 10^5$ M^{-1} s^{-1}) are large enough to account for obtaining relatively low polydispersities in the LRP of MA mediated by organo-cobalt complexes (Figure 1, 2).

$$\bullet MA-In + Co-MA \overset{k_{14}}{\rightleftharpoons} Co-MA-In + \bullet MA \quad (14)$$

$$\bullet MA_2 + Co-MA-In \overset{k_{15}}{\rightleftharpoons} Co-MA_2 + \bullet MA \quad (15)$$

$$\bullet MA_2 + Co-MA \overset{k_{16}}{\rightleftharpoons} Co-MA_2 + \bullet MA \quad (16)$$

During the early stage of the induction period complex **3** is exclusively observed concomitant with the decrease of (TMP)$Co^{II}\bullet$. This indicates that hydrogen atom transfer (eq 6) is preferred to addition of cyanoalkyl radical

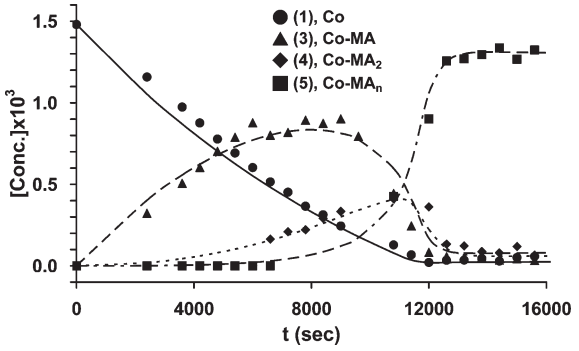

Figure 7. Experimental points and calculated lines for the concentrations of (TMP)$Co^{II}\bullet$ and organo-cobalt complexes during the polymerization process. ● = (TMP)$Co^{II}\bullet$ (**1**, Co), ▲ = (TMP)Co-CH(CO_2CH_3)CH_3 (**3**, Co-MA), ◆ = (TMP)Co-CH(CO_2CH_3)CH_2-CH(CO_2CH_3)CH_3 (**4**, Co-MA_2), ■ = (TMP)Co-CH(CO_2CH_3)CH_2-PMA (**5**, Co-MA_n). Initial concentrations: $[(TMP)Co^{II}\bullet]_i = 1.48 \times 10^{-3}$ M, $[V\text{-}70]_i = 2.00 \times 10^{-3}$ M, $[MA]_i = 0.14$ M. Parameters used in the kinetic simulations for reactions at 313 K are given in the Supporting Information.

(•C(CH_3)(R)CN, •In) with the MA monomer (eq 4). The observed ratio of rate constants for these two pathways shown in Scheme 2 is $k_1/k_2(313\ K) \approx 5 \times 10^{-4}$.

The sequence of the formation of organo-cobalt porphyrin species and the relative quantities provide evidence for the mechanistic model in Schemes 2 and 3. The occurrence of substantial amounts of (TMP)Co-CH(CO_2CH_3)CH_2-CH(CO_2CH_3)CH_3 (**4**) before the complete disappearance of (TMP)$Co^{II}\bullet$ (**1**) with a small quantity of (TMP)Co-CH(CO_2CH_3)CH_2-C(CH_3)(R)CN (**2**) indicates that **4** is formed through the homolytic dissociation of (TMP)Co-CH(CO_2CH_3)CH_3 (**3**) (Scheme 3(A)) and subsequent propagation with MA. However, in the analogous vinyl acetate system the organo-cobalt complex ((TMP)Co-CH(OC(O)CH_3)CH_2-CH(OC(O)CH_3)CH_3, Co-VAc_2) was only observed after the (TMP)$Co^{II}\bullet$ was exhausted. The late formation of Co-VAc_2 in the VAc system indicates that the monomer radical (•CH(OC(O)CH_3)CH_3) required for propagation with VAc was generated by an associative radical exchange (Scheme 3(B)) rather than homolytic dissociation (Scheme 3(A)). The different preferences for reaction pathways manifested in the organo-cobalt mediated LRP of MA and VAc are primarily the result of differences in the organo-cobalt dissociation equilibrium constants (K_d) which are dominated by the organic radical stability.

Regioselectivity for (TMP)Co−H addition with MA. Reaction of (TMP)Co−H with the double bond of methyl acrylate exclusively forms (TMP)Co-CH(CO_2CH_3)CH_3 which is the Markovnikov addition product. Porphyrin pyrrole nitrogen donors occupy all of the *cis*-coordination sites adjacent to the Co−H unit and block the concerted addition of (TMP)Co-H with CH_2=CH(CO_2CH_3). The lowest energy stepwise pathway in benzene probably involves hydrogen atom transfer to the olefin to give a radical pair that collapses to the organometallic complex (eq 17). The Markovnikov product is kinetically preferred by the hydrogen atom transfer

$$(TMP)Co-H + CH_2{=}CH(CO_2CH_3) \rightleftharpoons (TMP)Co\bullet\bullet CH(CO_2CH_3)CH_3 \rightleftharpoons (TMP)Co-CH(CO_2CH_3)CH_3 \quad (17)$$

(37) Goto, A.; Sato, K.; Tsujii, Y.; Fukuda, T.; Moad, G.; Rizzardo, E.; Tang, S. H. *Macromolecules* **2001**, *34*, 402–498.
(38) Kwak, Y.; Goto, A.; Fukuda, T.; Kobayashi, Y.; Yamago, S. *Macromolecules* **2006**, *39*, 4671–4679.
(39) Goto, A.; Ohno, K.; Fukuda, T. *Macromolecules* **1998**, *31*, 2809–2814.
(40) Kwak, T.; Goto, A.; Fukuda, T.; Yamago, S.; Ray, B. *Z. Phys. Chem.* **2005**, *219*, 283–293.

Table 2. C−H Bond Dissociation Energies to Form Radicals and the Energies of the SOMO of the Radicals Computed from DFT Calculation Using the B3LYP Functional and the 6-31G(d) Basis Set

C-H bond dissociation to form radical	C-H BDE[a] kcal mol^{-1}	RSE[b] kcal mol^{-1}	E(SOMO)[c] kcal mol^{-1}
CH_3-CH_3 ⟶ H· + ·CH_2−CH_3	98.3	0.0	0.0
CH_3-CH_2-O-C(=O)-CH_3 ⟶ H· + ·CH(−CH_3)−O−C(=O)−CH_3	93.1	-5.2	+10.7
CH_3-CH_2-C(=O)-O-CH_3 ⟶ H· + ·CH(−CH_3)−C(=O)−O−CH_3	88.3	-10.0	-19.5

[a] C−H BDE = C−H Bond Dissociation Energy. [b] RSE = Relative Stabilization Energy compared to the ethyl radical. [c] E(SOMO) = SOMO energy compared to the ethyl radical.

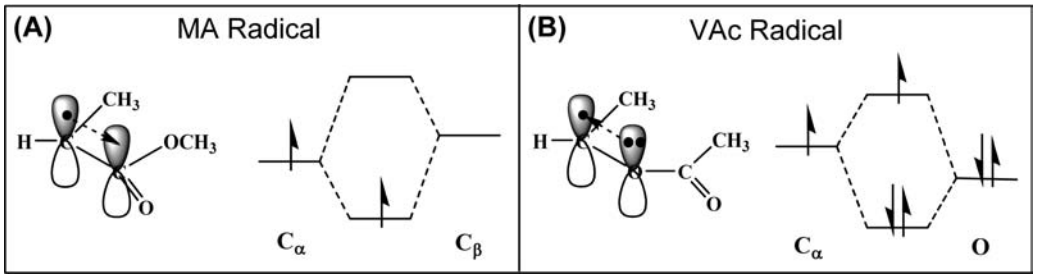

Figure 8. Influence on the energy of the SOMO of radicals by the π electron withdrawing group of methyl carboxylate in •$CH(CO_2CH_3)CH_3$ (A) and the π electron donating group of acetate in •$CH(OC(O)CH_3)CH_3$ (B).

mechanism because of the relative stability of the two possible intermediate radicals •$CH(CO_2CH_3)CH_3$ and •$CH_2CH_2CO_2CH_3$. The enthalpy of isomerization from •$CH(CO_2CH_3)CH_3$ to •$CH_2CH_2CO_2CH_3$ of +11 kcal mol^{-1} computed by DFT using the B3LYP functional and 6-31G(d) basic set[6] is consistent with the high selectivity for (TMP)Co-$CH(CO_2CH_3)CH_3$. The initially formed kinetic product (TMP)Co-$CH(CO_2CH_3)CH_3$ (**3**) is not observed to isomerize over extended periods of time in benzene and undoubtedly **3** is also the thermodynamic product. Exclusively Markovnikov addition is also observed reaction of (TMP)Co−H with VAc to form (TMP)Co-$CH(OC(O)CH_3)CH_3$. The polarity of organo-metal bonds (M^+R^-) provides an electronic effect that gives a thermodynamic preference for placing the electron withdrawing group on the α-carbon,[41] and the electronic effect more than compensates for the increased steric repulsion. (TMP)Co-$CH(CO_2CH_3)CH_3$ is thus both kinetically and thermodynamically preferred to (TMP)Co-$CH_2CH_2CO_2CH_3$.

Comparison of Thermodynamic and Kinetic Factors for Cobalt Porphyrin Mediated Radical Polymerization of MA and VAc. Thermodynamic and kinetic parameters for many of the steps in the (TMP)Co mediated polymerizations of methyl acrylate and vinyl acetate are heavily influenced by the electronic properties of radical species derived from MA and VAc. The energies for the SOMO and the relative radical stabilization energies for the parent radicals derived from MA (•$CH(CO_2CH_3)$-CH_3) and VAc (•$CH(OC(O)CH_3)CH_3$) from DFT calculations using the B3LYP functional and 6-31G(d) basis set are given in Table 2.

The difference in C−H bond dissociation energies for organic molecules is dominated by the relative stabilization energy of the organic radical fragments. The radical from VAc (•$CH(OC(O)CH_3)CH_3$) is stabilized (−5.2 kcal mol^{-1}) but the SOMO is raised in energy by +10.7 kcal mol^{-1} relative to •CH_2CH_3 while the MA radical (•$CH(CO_2CH_3)CH_3$) is more stabilized (−10.0 kcal mol^{-1}) and the energy of the SOMO lowered by −19.5 kcal mol^{-1} relative to the ethyl radical (Table 2, Figure 8). Delocalization of the unpaired electron to the π accepting -CO_2CH_3 group substantially lowers the energy of the SOMO but the π donor properties of the -$OC(O)CH_3$ unit raises the SOMO energy (Figure 8).

Radicals derived by adding a hydrogen atom to MA and VAc are both stabilized relative to •CH_2CH_3, but •$CH(CO_2CH_3)CH_3$ is stabilized by 4.8 kcal mol^{-1} more than •$CH(OC(O)CH_3)CH_3$ (Table 2). The difference in radical stabilities contributes directly to the difference in Co−R bond dissociation free energies which accounts for the much smaller Co−R dissociation constant for the (TMP)Co-$CH(OC(O)CH_3)CH_3$ (Co-VAc) compared to the MA derivative. The dissociation constant (K_d) of 1.15×10^{-10} (Table 1) at 333 K for Co−R bond homolysis of (TMP)Co-$CH(CO_2CH_3)CH_2$-P evaluated during the MA polymerization (eq 3, Figures 3 and 4) provides organic radical concentrations that are nearly ideal for controlling radical polymerization by dissociative RT (eq 1). The corresponding Co−R dissociation constant for the vinyl acetate derivative (TMP)Co-$CH(OC(O)CH_3)CH_2$-P ($K_{d(333\ K)} < 10^{-12}$) is too small to give organic radical concentrations required for useful rates of VAc polymerization by dissociative RT.

The π electron withdrawing property of the -CO_2CH_3 groups and π electron donation by -$OC(O)CH_3$ result in a dramatic stabilization of 30 kcal mol^{-1} for the SOMO energy of •$CH(CO_2CH_3)CH_3$ relative to that of •$CH(OC(O)CH_3)CH_3$ (Table 2). The greater stabilization of MA radical SOMO contributes to larger propagation constants for radical polymerization of MA compared to VAc ($k_{p(MA,\ 333\ K)} = 1.3 \times 10^4$ M^{-1} s^{-1}; $k_{p(VAc,\ 333\ K)} = 8 \times 10^2$ M^{-1} s^{-1})[5,6,35b,36] and improves the living character of (TMP)Co−R mediated radical polymerization of MA by

(41) Harvey, J. N. *Organometallics* **2001**, *20*, 4887–4895.

suppressing chain transfer events that are much more prominent for the high energy SOMO of vinyl acetate.

Summary

The reaction schemes for formation and transformation of organo-cobalt complexes in the cobalt porphyrin mediated methyl acrylate and vinyl acetate radical polymerizations are qualitatively the same, but differences in thermodynamic and kinetic parameters result in different propensities for the alternate reaction pathways. The dissociation equilibrium constant ($K_{d(333\ K)}$) for organo-cobalt complexes formed during the MA polymerization was determined as 1.15×10^{-10} at 333 K and the stronger Co−C bond in organo-cobalt derivatives of vinyl acetate results in a level of dissociation that is too small for evaluation of equilibrium constant by ^{1}H NMR ($K_{d(333\ K)} < 10^{-12}$). The ratio of the rate constants for the initiator radical ($\bullet C(CH_3)_2CN$) to add with monomer (eq 4) and transfer a hydrogen atom to (TMP)$Co^{II}\bullet$ (eq 6) (k_1/k_2) was evaluated as 2×10^{-3} for methyl acrylate LRP and 9×10^{-5} for vinyl acetate LRP at 333 K.[6] Kinetic simulations place the rate constant (333 K) for associative radical interchange at $\sim 7 \times 10^5\ M^{-1}\ s^{-1}$. The sequence in the formation of organo-cobalt complexes indicates that bond homolysis is important for the interconversion of organo-cobalt species formed in methyl acrylate LRP but associative radical exchange is the exclusive pathway for the transformation of organo-cobalt species in the LRP of vinyl acetate. The greater radical stabilization energy and lower energy of the SOMO for radicals derived from MA ($\bullet CH(CO_2CH_3)CH_3$) compared to VAc contribute to the observed better control of methyl acrylate LRP than that for vinyl acetate.

Experimental Section

Materials. Methyl Acrylate (Aldrich, 99%, 100 ppm MEHQ inhibitor) was stored in the refrigerator and vacuum distilled before use. The azo initiators, V-70 ($(((CH_3)_2(OCH_3)C(CH_2)C(CN)(CH_3))_2N_2$) and AIBN ($(((CH_3)_2(CN)C)_2N_2$), were purchased from Wako Chemicals U.S.A., Inc. and recrystallized using methanol for V-70 and ethanol for AIBN.[42] Cobalt Acetate was supplied by Fisher Scientific and used as received. Tetramesitylporphyrin (TMP)H_2 and cobalt(II)tetramesitylporphyrin ((TMP)$Co^{II}\bullet$) were synthesized following literature methods.[43,44] All Solutions of MA, (TMP)H_2, V-70, and AIBN were subjected to three freeze−pump−thaw cycles to remove any residual oxygen.

Analytical Techniques. Polymerization reactions are monitored by ^{1}H NMR spectra obtained on a Bruker AMX500 MHz NMR spectrometer at room temperature. Chemical shifts were calibrated relative to the solvent peak (deuterated benzene at 7.155 ppm, purchased from Cambridge Isotope Laboratory Inc.). The percent conversion was determined by intergrating the peaks corresponding to the vinyl protons of the monomer (5.0−6.4 ppm) and aliphatic protons of the polymer (1.4−2.8 ppm).

GPC analysis for PMA was made on a Shimadzu modular system, composed of a Polymer Laboratories 5.0 μm PLgel guard column (50 × 7.5 mm) followed by three linear PLgel columns (10^6, 10^4, and 5×10^2 Å) in an oven (CTO-10A), a UV detector (SPD-10AV) at 600 nm, and a differential refractive index detector (RID-10A), using THF as the eluent at 40 °C with a flow rate of 1 mL min^{-1}. This system was calibrated using narrow peak width polystyrene standards (Easical, preprepared polymer calibrants purchased from Polymer Laboratories) ranging from 580 to 7.5×10^6g mol^{-1}.

Polymerization Procedures. Aliquots of the (TMP)$Co^{II}\bullet$ and initiator (V-70 or AIBN) in C_6D_6 stock solutions were mixed to obtain desired ratios of radical to (TMP)$Co^{II}\bullet$ in a vacuum adapted NMR tube, and a measured volume of the C_6D_6 stock solution of MA was subsequently injected into the vacuum adapted tube containing (TMP)$Co^{II}\bullet$ and initiator (V-70 or AIBN) and subjected to three freeze−pump−thaw cycles to remove dissolved gases. The reaction tube and sample were then placed in a constant temperature bath (60.0 ± 0.1 °C or 40.0 ± 0.1 °C) and the progress of the polymerization followed by ^{1}H NMR.

One specific polymerization sample was prepared by mixing C_6D_6 solutions of (TMP)$Co^{II}\bullet$ (0.30 mL of 1.97×10^{-3} M), V-70 (0.05 mL of 0.016 M), and methyl acrylate (0.05 mL) in a vacuum adapted NMR tube and subjected to three freeze−pump−thaw cycles. The sample was placed in a 60.0 °C constant temperature bath, and the polymerization followed by ^{1}H NMR. Monomer conversion reached 51.94% in 120 min, and the number average molecular weight of the polymeric products was 41000 with polydispersity of 1.18. The solvent and unreacted monomer were then removed under vacuum, and the dried polymer products were dissolved in THF for the GPC analysis without further purification.

Acknowledgment. This research was supported by the Department of Energy Office of Basic Energy Science through grant DE-FG02-09ER16000 and the National Science Foundation through grant CHE 0809395.

Supporting Information Available: ^{1}H NMR spectrum analysis of **3**, **4**, **5**, comparison of the properties of V-70 and AIBN, and kinetic simulations for a representative polymerization process (shown in Figure 7). This material is available free of charge via the Internet at http://pubs.acs.org.

(42) Fukuda, T.; Ma, Y. -D.; Inagaki, H. *Macromolecules* **1985**, *18*, 17–26.
(43) Lindsey, J. S.; Wagner, R. W. *J. Org. Chem.* **1989**, *54*, 828–836.
(44) Woska, D. C; Xie, Z. D; Gridnev, A. A.; Ittel, S. D.; Fryd, M.; Wayland, B. B. *J. Am. Chem. Soc.* **1996**, *118*, 9102–9109.